Twelfth Quarterly Progress Report

October 1, 2004, through December 31, 2004

Speech Processors for Auditory Prostheses

NIH Contract N01-DC-2-1001

Submitted by

Donald K. Eddington
Massachusetts Institute of Technology
Research Laboratory of Electronics
Cambridge, MA

Barbara Herrmann
Massachusetts Eye and Ear Infirmary
Boston, MA

Charles C. Finley
University of North Carolina at Chapel Hill
Department of Otolaryngology
Chapel Hill, NC

1.0 Introduction

Work performed with the support of this contract is directed at the design, development, and evaluation of sound-processing strategies for auditory prostheses implanted in deaf humans. The investigators, engineers, audiologists and students conducting this work are from four collaborating institutions: the Massachusetts Institute of Technology (MIT), the Massachusetts Eye and Ear Infirmary (MEEI), Boston University (BU) and the University of North Carolina at Chapel Hill (UNC-CH). Major research efforts are proceeding in four areas: (1) developing and maintaining a laboratory-based, software-controlled, real-time stimulation facility for making psychophysical measurements, recording field and evoked potentials and implementing/testing a wide range of monolateral and bilateral sound-processing strategies, (2) refining the sound processing algorithms used in current commercial and laboratory processors, (3) exploring new sound-processing strategies for implanted subjects, and (4) understanding factors contributing to the wide range of performance seen in the population of implantees through psychophysical, evoked-response and fMRI measures.

This quarter's effort was directed at three areas: (1) measures of speech-reception, ITD sensitivity and localization in bilaterally-implanted subjects and (2) analysis of intracochlearly-recorded, electrically-evoked potentials (IEPs) recorded during single- and two-electrode stimulation conditions in a number of monolaterally-implanted subjects using the Clarion CII/HiFocus implant system and (3) modeling the aforementioned IEPs. In this QPR, we summarize the first steps in building models that explain unexpected characteristics of the IEPs recorded during two-electrode stimulation.

2.0 Hyperinteraction Measured with IEPs

Electrode interactions for *simultaneous* stimuli were estimated using intracochlearly-recorded, electrically-evoked potentials (IEPs) as described by Herrmann et al.(2003). The amplitude of the IEP (aIEP), defined as the difference between the amplitudes of the initial negative wave (N_1) and the following positive wave (P_2) responses, was measured for a suprathreshold probe pulse both alone and in the presence of a subthreshold masker. Figure 1 shows a sample of the control conditions used in the experiment. Condition E, where the aIEP was measured for a probe stimulus alone, served as the "no interaction" control. In conditions A and B, a simultaneous masker pulse was added to the *same* electrode as the probe, in-phase and out-of-phase with the probe pulse, respectively. These conditions serve as "complete interaction" controls, with maximum spatial overlap between masker and probe electric fields. Because the masker and probe stimuli are presented simultaneously to the same electrode, the aIEPs measured in conditions A, B and E fall along the IEP input-output (I/O) function (stars in Figure 1). Conditions C and D (not shown in Figure 1) serve as test conditions, where the probe and in- or out-of-phase masker pulses, respectively, are presented to different electrodes. Table I summarizes the five stimulus conditions.

Table I Masker/Probe Stimulus Conditions				
Condition	Probe Stimulus on Probe Electrode	Masker		Masker Phase re Probe
		Stimulus	Electrode	
A	●	●	Probe	In
B	●	●	Probe	Out
C	●	●	Masker	In
D	●	●	Masker	Out
E	●			

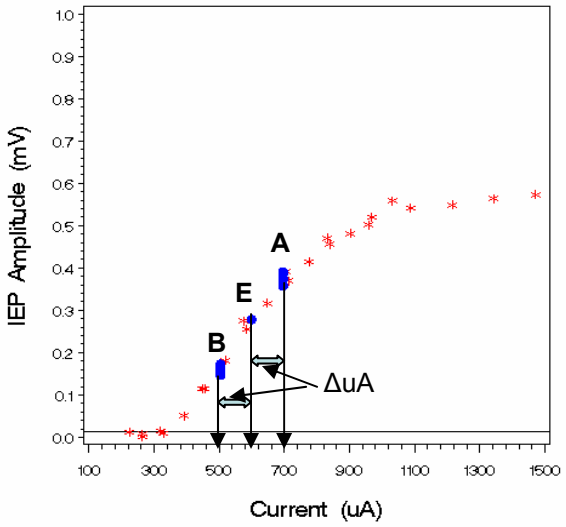

Figure 1. I/O function (stars) for one probe electrode plotted with aIEPs measured at 3 stimulus conditions (circles) used by the interaction procedure in a typical subject

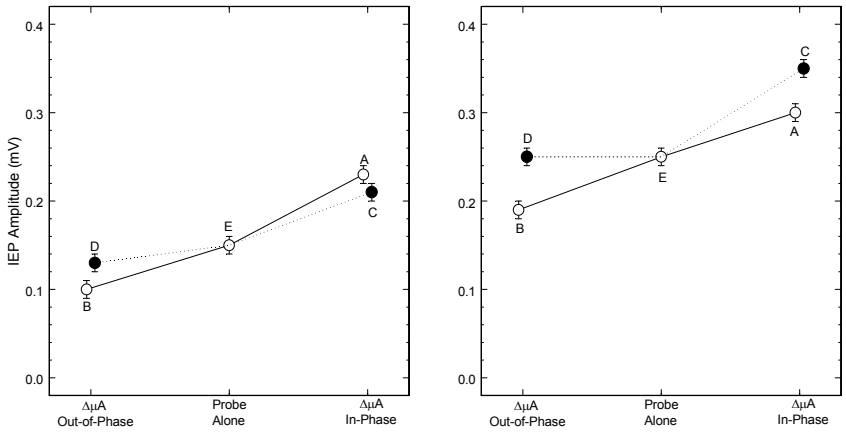

Figure 2. Examples illustrating two interaction patterns. The left panel illustrates interaction since the aIEP for conditions C and D (masker and probe on separate electrodes) differ significantly from the aIEP of condition E (probe only). The right panel illustrates an unexpected degree of interaction most often observed for in-phase maskers. Here the ΔuA stimulus on the masker electrode increases aIEP more than if the same change in current was applied directly to the probe electrode (i.e., the aIEP for Condition C is significantly greater than the aIEP for both Condition E and Condition A.

Figure 2 illustrates interaction analyses for two pairs of probe and masker electrodes. In the following discussion, $aIEP_X$ refers to the aIEP measured in condition X. The left panel of Figure 2 illustrates a case where interaction was present for both in- and out-of-phase maskers: $aIEP_C$ and $aIEP_D$ were each significantly different than $aIEP_E$. However, this interaction was not "complete:" $aIEP_C$ and $aIEP_D$ were not as different from $aIEP_E$ as the "complete interaction" controls $aIEP_A$ and $aIEP_B$, respectively. The right panel illustrates two other interaction cases. In this example, there was no interaction for an out of phase masker; $aIEP_D \sim aIEP_E$. For an in-phase masker, there was unexpected "hyperinteraction:" $aIEP_C$ was significantly greater than both $aIEP_E$ and $aIEP_A$. This was surprising because we expected the masker to maximally affect the response to the probe when both are delivered to same electrode (condition A).

Our IEP-measured simultaneous interaction results for three probe electrodes and nine maskers per electrode (Herrmann, Finley et al. 2003; Finley et al. 2004) showed that the likelihood of IEP interaction changed with the position of the probe electrode and the

leading phase of the masker stimulus. The apical and mid-region probe electrodes had a greater frequency of interaction than basal probe electrodes and the likelihood of interaction was greatest for maskers close to the probe and for apical maskers. Two unexpected types of interaction were observed: "hyperinteraction", as illustrated in Figure 2, where the effect of the masker was larger for condition C than for condition A and "inverse interaction" where the direction of the masker effect was opposite that expected. "Inverse" interaction occurred when an out-of-phase masker which was expected to decrease the amplitude of the probe IEP actually increased IEP amplitude (e.g., $aIEP_D > aIEP_E$). This type of interaction only occurred when the probe and the masker were at either end of the electrode array and likely reflects cross-turn coupling.

Our findings of simultaneous IEP interaction have some similarities to non-simultaneous IEP "neural excitation spread profiles" reported by Abbas et al. (2004) and Cohen et al. (2003) even though they were collected from a different cochlear implant (Clarion vs. Nucleus) and used a different IEP recording technique. Both reports show (1) the greatest effect of the masker near the probe stimulus and (2) maskers apical to the probe generally producing larger impact than basal maskers. While both studies report subjects with unusual excitation spread profiles, unexpected effects of the masker (like "hyperinteraction" and "inverse" interaction) are not reported by the Abbas et al. or Cohen et al. studies. This is likely due to the forward-masking technique they used to record the IEP which (because of the subtractions used to derive the probe response) makes it more difficult to see effects such as "hyperinteraction" or "inverse" interaction.

3.0 Electroanatomical models (EAMs) of the implanted cochlea

Because a model that successfully predicts the IEP-measured electrode interactions described in Section 2.0 would enable us to identify the peripheral mechanisms underlying the characteristics of those interactions, we decided to test a model developed in Eddington's laboratory for the rat to determine the extent it would predict (1) IEP waveforms measured in the rat and (2) the "hyperinteraction" we measured in our human subjects. If this model shows promise, we plan to develop a similar model based on human temporal bones.

Formulation of the model followed the methods developed and used by us to create previous human models and rat models (Girzon 1987; Whiten 2003). After the donor temporal bone is decalcified, sectioned, stained and cover-slipped, a set of digital color photos of every 5-μm thick histological slide that includes the cochlea, surrounding bone and/or auditory nerve in the internal auditory meatus is captured using a Neurolucida system that allows serial sections to be viewed and photographed under several microscope objectives, while maintaining a fixed coordinate system. The resulting two-dimensional (2D) serial images are registered (with the aid of a similar set of images photographed from the face of the temporal bone as it was sectioned) to form a three-dimensional (3D) structure that represents the complex, nonhomogeneous anatomy of the cochlea and auditory nerve. This structure is then "segmented" with homogeneous spatial regions being tagged to identify the tissue (e.g., bone and nerve), fluid (e.g.,

endolymph, perilymph, and extracellular) or material (e.g., electrode contact and electrode carrier) each represents. At this stage approximately 200 auditory-nerve fiber tracks distributed from base to apex are defined and the segmented structure then spatially sampled (e.g., Δx=6.25 μm, Δy=6.25 μm, Δz=5 μm) to generate a 3D matrix of volume elements (voxels). Each voxel is assigned electrical properties based on the tissue, fluid or material it represents. Current formulations ignore the capacitance of all tissues based on measures of tissue impedance showing that the resistive component dominates the reactance up to frequencies of 12.5 kHz (Geddes and Baker 1967; Spelman et al. 1982). The resulting 3D matrix represents the very complex electroanatomy of the implanted cochlea and can be used to compute the potential distribution produced in that structure by intracochlear stimulation.

A conjugant-gradient, finite-difference algorithm (Girzon 1987) is used to compute the potential (as a function of time) at each voxel for stimulating an arbitrary electrode configuration. The potentials along each of the model's nerve-fiber tracks are extracted and treated as that fiber's extracellular potential (as a function of time) during stimulation. These potentials are passed to a single-fiber model (25 nodes with cell body) of the mammalian auditory nerve developed by (Frijns 1995) that given the extracellular stimulus as a function of time, computes an estimate of the node potentials as a function of time.

In addition to estimating the spatio-temporal patterns of spike activity produced by intracochlear stimulation, the node-potential vs. time data is also used to predict the electrically-elicited IEP recorded by any intracochlear electrode pair. In the same way the potential-estimation routine can be used to predict the electric field during stimulation of an electrode, the potential distribution produced by the current flowing between any two neighboring fiber nodes can also be computed. By a applying a unit current between two point-sources spanning each fiber internode and computing the resulting potential distribution, a weight is determined for each model voxel that relates the relative potential amplitude at that voxel for a unit current at each internode of each fiber. A prediction of the IEP recorded at any intracochlear electrode is then computed by summing the appropriately-weighted, time-varying node potentials of all model fibers. Note that using these techniques, an IEP can be computed for arbitrary stimulation and recording electrode configurations.

4.0 An EAM of the implanted cochlea accurately predict IEP waveforms

Because the waveforms of intracochlear-recorded, electrically-evoked potentials (IEPs) are a function of the complex spatial and temporal distribution of the spike activity generated by electric stimulation, they represent one of the best benchmarks against which to test our EAMs. A large set of existing recordings of IEPs made in 13 Long-Evans rats by our group, provides a unique opportunity to test an EAM of the rat auditory periphery we formulated using the techniques summarized in Section 3.0 and (Girzon 1987; Whiten 2003).

The model includes the cochlea, surrounding bone with the internal auditory meatus, auditory nerve and the cochlear nucleus in the brainstem. Spatial resolution for the rat model is 6.25 µm by 6.25 µm by 5 µm. Model electrodes are positioned to represent the five electrodes implanted in each rat and distributed over the entire cochlear length. In the rat, IEPs are recorded monopolarly at unstimulated electrodes and referenced to subcutaneous needle electrodes in the ipsilateral hip. Monopolar stimuli are delivered between one intracochlear electrode and a subcutaneous needle electrode in the ipsilateral pinna.

Figure 3 shows an example of the IEP waveforms recorded for apical and basal stimulation in one animal and the IEP waveforms predicted by the rat model. The dramatic difference in waveforms between apical and basal stimulations observed in the rat recordings is predicted by the model. The time between the first minimum and first maximum for apical stimulation is somewhat longer than predicted by the model (0.18 ms vs. 0.12 ms). However, for basal stimulation, the model prediction was closer (0.12 ms for the recorded waveform and 0.13 ms for the model prediction). The remarkable correspondence between the measured and predicted IEP waveforms gives us confidence that models based on the techniques described in Section 3.0 can be used to formulate a human model that accurately predicts the spatio-temporal patterns of auditory-nerve activity elicited by electric stimulation.

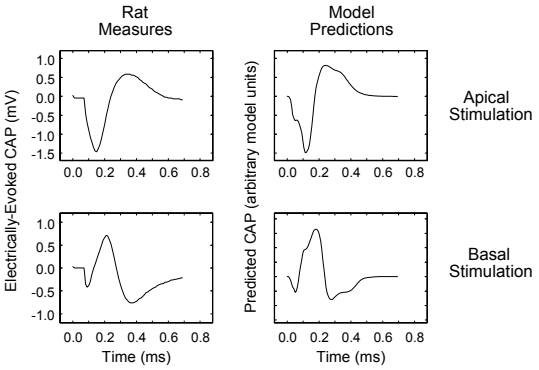

Figure 3. Recorded (left column) and model-predicted (right column) eIEP waveforms elicited by monopolar apical (top row) and basal (bottom row) stimulation. Recorded waveforms are the result of averaging 1000 responses (bandwidth: 3 Hz to 30 kHz; sample rate: 100 kHz). Stimuli were 10-µApp, sinusoidal, 1-kHz tone pips (2-cycle rise/fall times and 5-cycle plateau).

5.0 An existing electroanatomical model predicts the hyperinteraction measured using IEPs.

Figure 4 plots predictions of an electroanatomical model (Girzon 1987; Whiten 2003) for stimulus/recording conditions similar to the in-phase conditions shown in the right panel of Figure 2 (probe-masker electrode separation ≈1mm) for the A, E and C stimulus configurations. The model is based on the temporal bone of a patient implanted during life and includes the complex, nonhomogeneous structure of the implanted cochlea and a population of model nerve fibers distributed along the length of the cochlea. Model inputs are stimulus pulses at specified intracochlear electrode positions. The model predicts the distribution of spike activity on the array of auditory nerve fibers and the resulting compound action potentials (CAPs) recorded at specified (unstimulated) electrode positions.

In the case of Figure 4, the magnitude of the N_1 wave of the CAP is plotted as a function of the probe stimulus level with the subthreshold masker level held constant at 6 dB below threshold. For probe levels up to 0.4 model units (mu), the N_1 magnitudes elicited by C-condition stimuli are the same or below those elicited by A-condition stimuli (incomplete or complete interaction). At higher stimulus levels the response magnitudes become larger for condition C than for condition A, predicting the hyperinteraction shown for the in-phase masker and probe observed in the right panel of Figure 2.

While the IEP recorded at the electrode at 300° will be a very complex function of the nonhomogeneous electrical structure of the cochlea, it is possible to identify some important trends from the model-predicted threshold plotted as a function of longitudinal cochlear position shown in Figure 5. For example, it is clear that, except for a few fibers

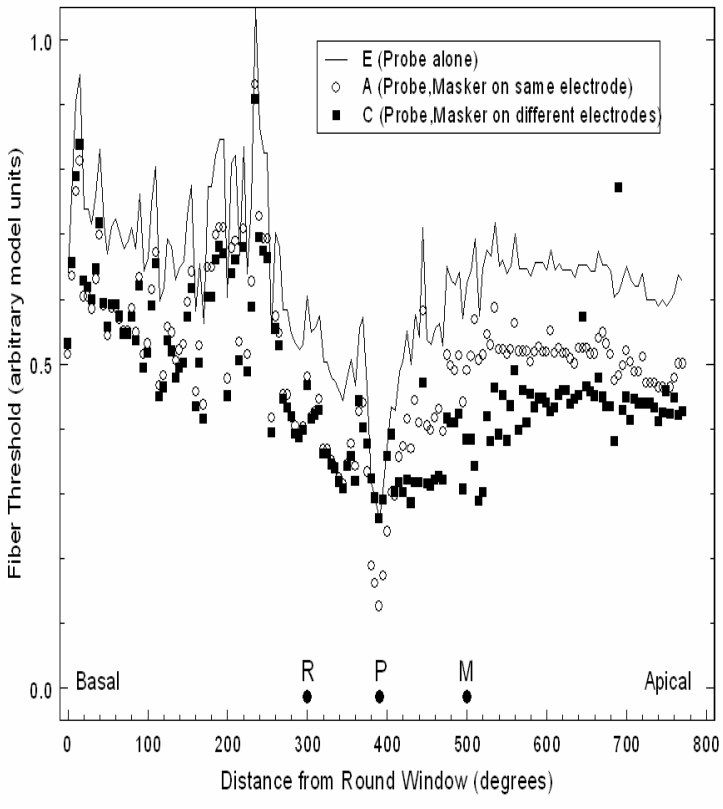

Figure 5. Plot of predicted fiber threshold as a function of fiber position for three stimulus conditions: probe alone (E, line), probe and masker both applied to the probe electrode (A, open circles), and probe and masker applied to different electrodes (C, filled squares). The intracochlear probe (P), masker (M) and recording (R) electrodes are located at 390°, 500° and 300° respectively. Masker level is 6 dB below the masker threshold.

near the probe electrode (P in Figure 5), fibers tend to have a lower threshold in condition C (masker stimulus delivered to electrode M at approximately 500^{o}) than in conditions A (masker on electrode P) or E (no masker). This is especially true of fibers apical to the probe electrode for this apical-masker configuration. As a result, for stimulus levels above 0.3 model units, fibers will tend to be recruited at lower stimulus levels in condition C than in the conditions A and E, consistent with the hyperinteraction shown in Figure 2. These results suggest that the hyperinteraction is probably due to the increased sensitivity of fibers to the probe electrode as a result of partial depolarization by the masker stimulus in the C stimulus condition.

Because this electroanatomical model is successful in explaining an unexpected simultaneous electrode interaction phenomenon observed using IEP, we anticipate that it will also be useful in understanding other types of electrode interactions. These results together with those of Section 4.0 lead us to begin working on an EAM formulated using a human temporal bone.

6.0 Future Work

We are conducting binaural psychophysical testing of two subjects who have used a monolateral implant for at least 6 months and then bilateral stimulation for about 6 weeks. We continue to measure relative interaural pitch, fusion, ITD-JND, speech reception, localization and binaural interactions in electrically-evoked brain stem responses as a function of time in the three bilaterally-implanted subjects described in earlier QPRs. We are also evaluating split-spectrum processors using asynchronous sound processors. These data, together with results from current testing designed to determine the cues these subjects use in localization tasks will be reported in our next and last QPR.

We are in the process of using existing EAMs to explore the characteristics of IEP-measured, simultaneous electrode interaction and plan to extend the measures and analyses to nonsimultaneous electrode interaction.

7.0 References

Abbas, P. J., M. L. Hughes, C. J. Brown, C. A. Miller and H. South (2004). "Channel interaction in cochlear implant users evaluated using the electrically-evoked compound action potential." Audiology and Neuro-Otology **9(4), 203-213.**(4): 203-213.

Cohen, L. T., L. M. Richardson, E. Saunders and R. S. Cowan (2003). "Spatial spread of neural excitation in cochlear implant recipients: comparison of improved ECAP method and psychophysical forward masking." Hear Res **179**(1-2): 72-87.

Finley, C. C., B. Herrmann and D. K. Eddington (2004). Speech processors for auditory prostheses: tenth quarterly progress report. Bethesda, Neural Prosthesis Program, National Institutes of Health.

Frijns, J. H. M. (1995). Cochlear implants: a modelling approach. Faculteit der Godgeleerdheid. Eindhoven, Rijksuniversiteit te Leiden**:** 184.

Geddes, L. A. and L. E. Baker (1967). "The specific resistance of biological material--a compendium of data for the biomedical engineer and physiologist." Med Biol Eng **5**(3): 271-93.

Girzon, G. (1987). Investigation of Current Flow in the Inner Ear During Electrical Stimulation of Intracochlear Electrodes. Department of Electrical Engineering and Computer Sciences. Cambridge, MA, M.I.T.

Herrmann, B., C. C. Finley and D. K. Eddington (2003). Speech processors for auditory prostheses: eighth quarterly progress report. Bethesda, Neural Prosthesis Program, National Institutes of Health.

Spelman, F. A., B. M. Clopton and B. E. Pfingst (1982). "Tissue impedance and current flow in the implanted ear. Implications for the cochlear prosthesis." Ann Otol Rhinol Laryngol Suppl **98**: 3-8.

Whiten, D. M. (2003). Threshold Predictions Based on an Electro-anatomical Model of the Cochlear Implant. Electrical Engineering and Computer Science. Cambridge, Massachusetts Institute of Technology**:** 141.